Article

Structures and Stabilities of Carbon Chain Clusters Influenced by Atomic Antimony

Zhenjun Song [1,2], Xiji Shao [3], Wei Wu [4], Zhenzhong Liu [5], Meiding Yang [1,*], Mingyue Liu [1,*] and Hai Wang [6,7,*]

1 School of Pharmaceutical and Chemical Engineering, Taizhou University, Taizhou 318000, China
2 Department of Chemistry, Tongji University, Shanghai 200092, China
3 School of Intelligent Engineering, Shaoguan University, Shaoguan 512005, China
4 Department of Physics and Astronomy, London Centre for Nanotechnology, University College London, London WC1E 6BT, UK
5 Research Institute of Zhejiang University-Taizhou, Zhejiang University, Taizhou 318000, China
6 Key Laboratory of Yunnan Provincial Higher Education Institutions for Organic Optoelectronic Materials and Devices, Kunming University, Kunming 650214, China
7 Yunnan Key Laboratory of Metal-Organic Molecular Materials and Devices, Kunming University, Kunming 650091, China
* Correspondence: yangmd@tzc.edu.cn (M.Y.); liumingyue0820@126.com (M.L.); hai.wang.ucl@gmail.com (H.W.)

Abstract: The C-C bond lengths of the linear magnetic neutral C_nSb, C_nSb^+ cations and C_nSb^- anions are within 1.255–1.336 Å, which is typical for cumulene structures with moderately strong double-bonds. In this report, we found that the adiabatic ionization energy (*IE*) of C_nSb decreased with n. When comparing the $IE \sim n$ relationship of C_nSb with that of pure C_n, we found that the latter exhibited a stair-step pattern ($n \geq 6$), but the $IE \sim n$ relationship of C_nSb chains took the shape of a flat curve. The *IE*s of C_nSb were lower than those of corresponding pure carbon chains. Different from pure carbon chains, the adiabatic electron affinity of C_nSb does not exhibit a parity effect. There is an even-odd alternation for the incremental binding energies of the open chain C_nSb (for $n = 1–16$) and C_nSb^+ ($n = 1–10$, when $n > 10$, the incremental binding energies of odd (n) chain of C_nSb^+ are larger than adjacent clusters). The difference in the incremental binding energies between the even and odd chains of both C_nSb and pure C_n diminishes with the increase in n. The incremental binding energies for C_nSb^- anions do not exhibit a parity effect. For carbon chain clusters, the most favorable binding site of atomic antimony is the terminal carbon of the carbon cluster because the terminal carbon with a large spin density bonds in an unsaturated way. The C-Sb bond is a double bond with Wiberg bond index (WBI) between 1.41 and 2.13, which is obviously stronger for a carbon chain cluster with odd-number carbon atoms. The WBI of all C-C bonds was determined to be between 1.63 and 2.01, indicating the cumulene character of the carbon chain. Generally, the alteration of WBI and, in particular, the carbon chain cluster is consistent with the bond length alteration. However, the shorter C-C distance did not indicate a larger WBI. Rather than relying on the empirical comparison of bond distance, the WBI is a meaningful quantitative indicator for predicting the bonding strength in the carbon chain.

Keywords: carbon cluster; stability; antimony; parity effect; even-odd alteration

1. Introduction

Small magnetic carbon clusters and related carbon-based materials have attracted much attention on the account of their important role in astrophysics, terrestrial processes, electronic spintronics, catalysis, and chemical engineering [1–5]. A deep understanding of the carbon nanostructure with adjustable bonding should facilitate the designing and synthesizing of size- and morphology-controlled carbon-based functional materials [6–9]. Previous theoretical and experimental studies have revealed that small carbon clusters

are mainly of a linear structure [10–12]. The pure carbon clusters are ascertained to be intermediate in the production of diamonds, silicon carbine films, and a variety of chemical systems involving hydrocarbons [13–15]. Transition-metal doping for hybridization is an effective way to adjust the performance and electronic properties of nanomaterials [16–20]. In the interstellar medium, the reactivity of small carbon clusters is forfeited by quasi-collisionless conditions, and carbon atoms take the highly thermally stable, albeit highly reactive, form linear chains. When these metastable carbon chains encounter heteroatoms such as sulfur, oxygen, hydrogen, and nitrogen, they form more stable complexes.

Mass spectrometry is useful for detecting pure and doped carbon clusters with high stabilities. Theoretical studies of the linear carbon clusters show that doped by different heteroatom X, CnX/CnX$^+$/CnX$^-$ clusters have different parity effects in their stabilities [21–23]. Zhan and Iwata have used more sophisticated post-HF methods, including Møller-Plesset2 (MP2), MP4SDTQ, and the QCISD(T) method with different basis set to study the properties of CnN$^-$ and CnP$^-$ [24,25]. Zheng et al. produced cluster anions CnN$^-$ and CnP$^-$ from the laser ablation of appropriate samples and studied them by TOF mass spectrometry [26,27]. Small, doped carbon clusters have been extensively investigated theoretically and experimentally. Theoretical methods have been useful for studying heavier-atom-doped carbon clusters. Recently, theoretical work for lead [28], gallium [29], indium [30], gold [31], and tantalum [32] doped carbon clusters has been conducted. With the electronegativity modulation of heteroatom X, the parity effect in CnX may undergo dramatic changes. Their geometries, electronic structures, and bonding of small metal carbide clusters, such as antimony-doped carbon clusters, are yet to be determined systematically. In this paper, we report a density-functional-theory (DFT) study of the linear CnSb, CnSb$^+$, and CnSb$^-$ clusters.

2. Results and Discussion

2.1. Structural Optimization

Tables 1–3 present the optimized bond lengths obtained at the B3LYP/6-31G(d) level, while Figures 1–6 analyzed the C-C and C-Sb bond lengths. Tables 4–6 summarize the calculated total energies E_n of optimized structures, differential energies ΔE_n, binding energies BE, incremental binding energies ΔE^{I}, dipole moments, and rotational constants. As shown in Figure 1, we can find that the C-C bond lengths of neutral C_nSb are within the range of 1.270–1.304 Å, exhibiting the character of both double-bonds (C-C bond length of ethylene is computed to be 1.331 nm by using B3LYP/6-31G(d)) and triple-bonds (C-C bond length of acetylene 1.205 Å by B3LYP/6-31G(d)); The C-Sb bond length of neutral C_nSb is within the range of 1.941 Å to 1.968 Å. The C-C bond length alteration (BLA) of neutral C_nSb is obvious and tends to be irregular in the vicinity of Sb. For C_nSb$^+$ clusters, the C-C bond lengths are within a range from 1.259 Å to 1.334 Å, C-Sb bond lengths are in a range from 1.889 Å to 2.009 Å. The optimized BLA of corresponding C-C and C-Sb showed diverse tendencies compared with that of neutral C_nSb. The odd C_nSb$^+$ chains also have a significant BLA effect; instead of being weakened and irregular C-C bond length, the C-C BLA near the antimony atom is slightly enhanced, which is markedly different from the corresponding neutral ones. The C-C bond lengths of C_nSb$^-$ anions are within a range from 1.255 Å to 1.336 Å, and C-Sb bond lengths are within a range from 1.889 Å to 2.014 Å; the fluctuation trend of the BLA effect in even C_nSb$^-$ anions have the same tendencies with that of neutral C_nSb; different from neutral C_nSb, odd C_nSb$^-$ anions also have a distinct BLA effect, and this effect is more obvious than C_nSb$^+$ cations. Unlike the C_nSb$^+$ and C_nSb, the C-Sb bond lengths of even C_nSb$^-$ anions are larger than the adjacent odd cluster anions, as depicted in Figure 5. We can preliminarily infer from C-C BLA and C-Sb BLA that the antimony atom of even C_nSb$^+$ and odd C_nSb$^-$ might combine with the carbon clusters more firmly than adjacent clusters (this speculation can be proved roughly right for small clusters by our calculation on their dissociation channels). When comparing the BLA of neutral and charged antimony-doped carbon chains with that of pure carbon chains, it is easy to deduce that through doping the antimony element, the properties of carbon

clusters have been changed to a certain extent (Figures 1 and 2). The C-C bond lengths are within the range of 1.255 Å–1.336 Å, typical for cumulene structures with moderately strong double-bonds. On the other hand, the clear alternation in C-C distances suggests that there is a substantial contribution of polyacetylenic valence-bond structures with an alternating triple and single C-C bond.

**Table 1.** Optimized bond lengths (Å) for neutral C_nSb at b3lyp/6-31G(d) theoretical level.

CSb	1.888															
C2Sb	1.300	1.941														
C3Sb	1.301	1.296	1.949													
C4Sb	1.291	1.304	1.277	1.941												
C5Sb	1.294	1.297	1.280	1.288	1.946											
C6Sb	1.291	1.301	1.271	1.295	1.277	1.949										
C7Sb	1.292	1.299	1.274	1.288	1.282	1.286	1.945									
C8Sb	1.291	1.301	1.271	1.293	1.272	1.296	1.276	1.956								
C9Sb	1.291	1.300	1.272	1.289	1.276	1.285	1.284	1.285	1.947							
C10Sb	1.290	1.301	1.270	1.293	1.272	1.292	1.272	1.297	1.275	1.960						
C11Sb	1.291	1.300	1.272	1.290	1.275	1.287	1.278	1.284	1.286	1.284	1.949					
C12Sb	1.290	1.301	1.270	1.293	1.272	1.292	1.272	1.293	1.271	1.298	1.274	1.964				
C13Sb	1.291	1.300	1.271	1.291	1.274	1.288	1.277	1.286	1.280	1.283	1.287	1.283	1.951			
C14Sb	1.290	1.302	1.270	1.293	1.271	1.293	1.272	1.293	1.272	1.294	1.271	1.300	1.273	1.966		
C15Sb	1.290	1.301	1.271	1.291	1.274	1.289	1.276	1.287	1.278	1.285	1.281	1.282	1.288	1.282	1.952	
C16Sb	1.290	1.302	1.270	1.294	1.271	1.293	1.271	1.293	1.272	1.294	1.271	1.295	1.270	1.300	1.273	1.968

Table 2. Optimized bond length (Å) for C_nSb^+ cations at b3lyp/6-31G(d) theoretical level.

CSb	1.963															
C2Sb	1.326	1.889														
C3Sb	1.334	1.270	2.009													
C4Sb	1.315	1.277	1.300	1.891												
C5Sb	1.321	1.272	1.302	1.264	1.995											
C6Sb	1.311	1.276	1.291	1.268	1.301	1.894										
C7Sb	1.315	1.276	1.293	1.264	1.303	1.265	1.985									
C8Sb	1.308	1.278	1.290	1.266	1.295	1.266	1.303	1.896								
C9Sb	1.311	1.278	1.290	1.268	1.295	1.264	1.302	1.267	1.979							
C10Sb	1.306	1.279	1.289	1.267	1.295	1.263	1.298	1.265	1.304	1.897						
C11Sb	1.309	1.280	1.288	1.270	1.292	1.267	1.296	1.265	1.302	1.268	1.976					
C12Sb	1.304	1.281	1.287	1.268	1.294	1.264	1.298	1.262	1.300	1.264	1.304	1.898				
C13Sb	1.307	1.282	1.286	1.271	1.290	1.269	1.293	1.267	1.296	1.266	1.301	1.269	1.973			
C14Sb	1.303	1.283	1.286	1.270	1.292	1.265	1.297	1.262	1.300	1.260	1.301	1.264	1.305	1.897		
C15Sb	1.305	1.283	1.285	1.272	1.289	1.270	1.292	1.269	1.293	1.268	1.295	1.266	1.300	1.270	1.971	
C16Sb	1.302	1.284	1.285	1.271	1.291	1.266	1.296	1.263	1.300	1.260	1.302	1.259	1.303	1.263	1.306	1.898

Table 3. Optimized bond length (Å) for C_nSb^- anions at b3lyp/6-31G(d) theoretical level.

CSb	1.952															
C2Sb	1.280	2.014														
C3Sb	1.278	1.326	1.924													
C4Sb	1.273	1.336	1.260	2.000												
C5Sb	1.273	1.326	1.262	1.314	1.921											
C6Sb	1.273	1.329	1.256	1.323	1.261	1.997										
C7Sb	1.272	1.326	1.256	1.315	1.263	1.311	1.919									
C8Sb	1.273	1.326	1.257	1.317	1.258	1.319	1.262	1.994								
C9Sb	1.273	1.325	1.256	1.316	1.257	1.313	1.264	1.310	1.917							
C10Sb	1.274	1.324	1.257	1.314	1.259	1.314	1.259	1.317	1.263	1.992						
C11Sb	1.273	1.324	1.256	1.315	1.256	1.314	1.257	1.312	1.263	1.310	1.914					
C12Sb	1.275	1.322	1.258	1.312	1.259	1.312	1.260	1.311	1.260	1.315	1.264	1.990				
C13Sb	1.274	1.322	1.256	1.314	1.256	1.314	1.256	1.314	1.257	1.312	1.263	1.310	1.913			
C14Sb	1.276	1.321	1.258	1.312	1.259	1.311	1.260	1.310	1.261	1.310	1.261	1.314	1.265	1.987		
C15Sb	1.275	1.321	1.257	1.313	1.257	1.314	1.256	1.315	1.255	1.315	1.256	1.312	1.262	1.310	1.912	
C16Sb	1.276	1.320	1.258	1.311	1.260	1.310	1.260	1.310	1.261	1.309	1.261	1.309	1.262	1.312	1.266	1.985
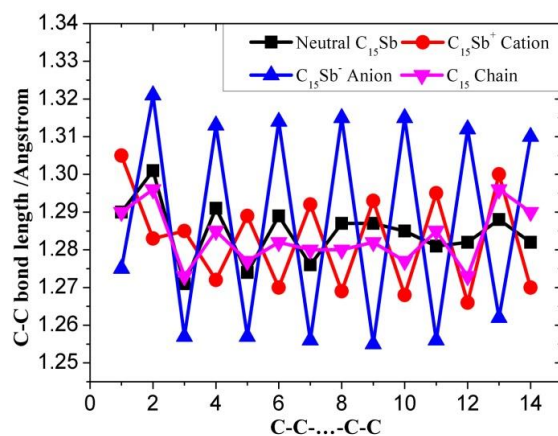
Figure 1. C-C bond length alteration of neutral $C_{15}Sb$, $C_{15}Sb^+$ cation, $C_{15}Sb^-$ anion, and pure carbon chain C_{15} as a function of number of carbon atoms.
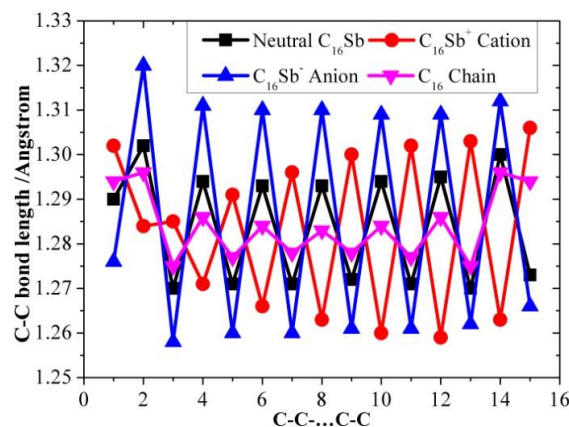
Figure 2. C-C bond length alteration of neutral $C_{16}Sb$, $C_{16}Sb^+$ cation, $C_{16}Sb^-$ anion, and pure carbon chain C_{16} as a function of number of carbon atoms.
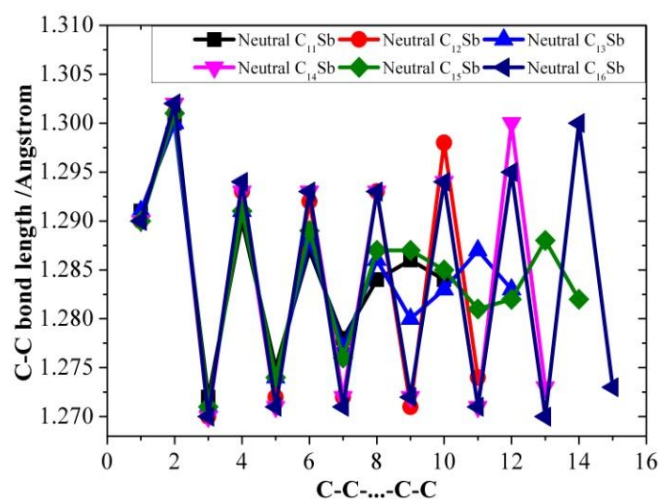
Figure 3. C-C bond length alteration of neutral C_nSb (n = 11–16) as a function of number of carbon atoms.
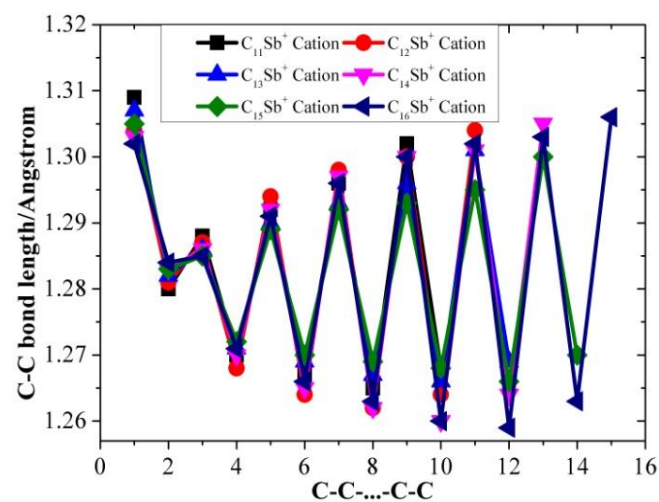

Figure 4. C-C bond length alteration of C_nSb^+ cations (n = 11–16) as a function of number of carbon atoms.
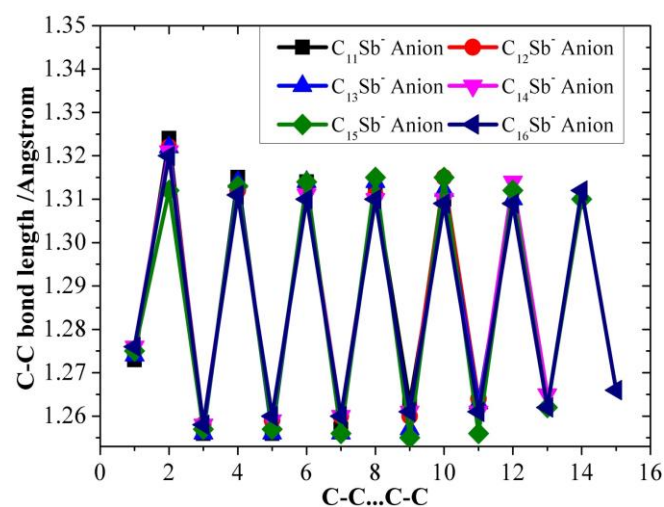

Figure 5. C-C bond length alteration of C_nSb^- anions (n = 11–16) as a function of number of carbon atoms.
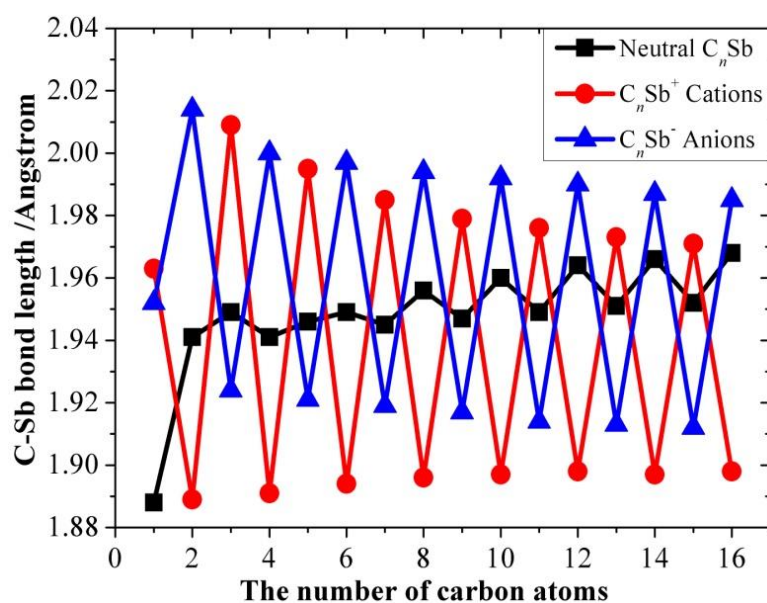
Figure 6. C-Sb bond length of neutral C$_n$Sb, C$_n$Sb$^+$ cation, and C$_n$Sb$^-$ anion as a function of number of carbon atoms.

Table 4. The total energies E_n, differential energies ΔE_n, incremental energies ΔE^{I}, binding energies BE, adiabatic ionization energies IE, adiabatic electron affinities EA, dipole moments, and rotational constants (RC) of neutral C$_n$Sb.

C$_n$Sb	E_n (a. u.)	ΔE_n (a. u.)	BE (a. u.)	ΔE^{I} (kcal/mol)	IE (kcal/mol)	EA (kcal/mol)	μ (debye)	RC (MHz)
1	−43.35455		0.10241		212.4	69.2	3.13	12990
2	−81.48162	−38.12707	0.37201	169.2	196.3	62.6	5.57	3497
3	−119.56561	−38.08399	0.59853	142.1	196.1	72.1	5.36	1519
4	−157.65877	−38.09316	0.83422	147.9	187.7	72.9	7.46	821
5	−195.74409	−38.08532	1.06207	143.0	186.3	78.7	7.10	496
6	−233.83823	−38.09414	1.29874	148.5	183.9	76.7	8.98	326
7	−271.91968	−38.08145	1.52272	140.5	179.1	83.0	8.75	227
8	−310.00802	−38.08834	1.75359	144.9	176.1	84.1	10.39	165
9	−348.09409	−38.08607	1.98219	143.4	173.8	86.2	10.31	125
10	−386.18172	−38.08763	2.21235	144.4	172.1	87.5	11.74	97
11	−424.26787	−38.08615	2.44103	143.5	169.5	88.6	11.78	77
12	−462.35529	−38.08742	2.67098	144.3	169.2	89.5	13.04	62
13	−500.44149	−38.08620	2.89971	143.5	166.2	90.5	13.19	51
14	−538.52879	−38.0873	3.12954	144.2	166.8	92.4	14.30	42
15	−576.61521	−38.08642	3.35849	143.7	163.5	92.0	14.53	36
16	−614.70241	−38.08720	3.58822	144.2	164.8	94.2	15.51	30

Table 5. The total energies E_n, differential energies ΔE_n, incremental energies ΔE^{I}, binding energies (BE), dipole moments (μ), and rotational constants (RC) of C_nSb^+ cations.

C_nSb^+	E_n (a. u.)	ΔE_n (a. u.)	BE (a. u.)	ΔE^{I} (kcal/mol)	μ(Debye)	RC (MHz)
1	−43.01612		−0.23602		1.08	12013
2	−81.16886	−38.15274	0.05925	0.29527	2.68	3584
3	−119.25339	−38.08453	0.28631	0.22705	0.85	1474
4	−157.35996	−38.10657	0.53541	0.24911	2.26	835
5	−195.44758	−38.08762	0.76556	0.23014	0.52	489
6	−233.54567	−38.09809	1.00618	0.24063	1.97	331
7	−271.63483	−38.08916	1.23787	0.23169	0.43	226
8	−309.72820	−38.09337	1.47377	0.2359	1.89	167
9	−347.81792	−38.08972	1.70602	0.23225	0.48	124
10	−385.90836	−38.09044	1.93899	0.23297	0.83	98
11	−423.99872	−38.09036	2.17188	0.2329	0.65	77
12	−462.08689	−38.08817	2.40258	0.23069	1.99	62
13	−500.17791	−38.09102	2.63613	0.23355	0.87	51
14	−538.26446	−38.08655	2.86521	0.22908	2.06	43
15	−576.35619	−38.09173	3.09947	0.23426	1.11	36
16	−614.44148	−38.08529	3.32729	0.22782	2.10	31

Table 6. The total energies E_n, differential energies ΔE_n, incremental energies ΔE^{I}, binding energies BE, dipole moments (μ), and rotational constants (RC) of C_nSb^- anions.

C_nSb^-	E_n (a. u.)	ΔE_n (a. u.)	BE (a. u.)	ΔE^{I} (kcal/mol)	μ (Debye)	RC (MHz)
1	−43.46493		0.21279		5.50	12153
2	−81.58147	−38.11654	0.47186	0.25908	8.89	3348
3	−119.68068	−38.09921	0.7136	0.24174	9.78	1528
4	−157.77531	−38.09463	0.95076	0.23715	13.03	800
5	−195.86996	−38.09465	1.18794	0.23718	13.52	496
6	−233.96096	−38.09100	1.42147	0.23353	16.53	321
7	−272.05265	−38.09169	1.65569	0.23422	16.93	227
8	−310.14274	−38.09009	1.88831	0.23262	19.74	163
9	−348.23223	−38.08949	2.12033	0.23202	20.16	125
10	−386.32214	−38.08991	2.35277	0.23243	22.76	96
11	−424.41010	−38.08796	2.58326	0.23049	23.26	77
12	−462.49915	−38.08905	2.81484	0.23158	25.04	62
13	−500.58704	−38.08789	3.04526	0.23042	26.30	51
14	−538.67748	−38.09044	3.27823	0.23296	28.52	42
15	−576.76336	−38.08588	3.50664	0.22841	29.33	36
16	−614.85418	−38.09082	3.73999	0.23335	31.33	30

We mainly focused on the linear carbon chain clusters initially because many reported carbon clusters mainly adopt a linear shape as the ground state structure. For the antimony-

doped larger carbon clusters (n > 10), we conducted density functional calculations to obtain the energies of ring structures. The total energies of $C_{11}Sb$ and $C_{14}Sb$ with a ring structure are 0.35 and 0.11 eV higher in energy than linear $C_{11}Sb$ and $C_{14}Sb$ clusters, while $C_{12}Sb$, $C_{13}Sb$, $C_{15}Sb$, and $C_{16}Sb$ clusters with a ring structure are −0.14, −0.57, −0.53, and −0.83 eV lower in energy. Although the linear carbon cluster is not always the global minima in the potential surface, the linear carbon clusters possess a practical significance that the reactivity of carbon clusters increases dramatically with the increasing number of consecutive cumulene-like double bonds, and the linear carbon clusters can be formed in space-confined nanotube materials [33–35]. The linear carbon chain cluster with different lengths and doping atoms is a special allotrope type of carbon material different from graphite, diamond, graphene, carbon nanotubes, and fullerenes.

We made comparisons between 6-31G(d) and def2-TZVP basis sets for selected structural parameters, C-Sb stretching frequencies, and HOMO-LUMO gaps in Table 7. The C-C bonds adjacent antimony atoms of C_4Sb, C_5Sb, C_6Sb, $C_{10}Sb$, and $C_{11}Sb$ show only slight differences less than 0.011 Å, and the C-Sb bond distances are almost the same through using def2-TZVP and 6-31G(d) basis sets. C-Sb stretching frequencies tend to show negligible differences for the larger $C_{11}Sb$ and $C_{12}Sb$. Although the C-Sb stretching frequency differences for C_4Sb and C_5Sb, it is slightly larger (6.2 cm^{-1} and 3.9 cm^{-1}) under different basis sets, and we can clearly recognize that the theoretically predicted vibration modes are the same by comparing normal coordinates. The HOMO-LUMO gaps for C_4Sb, C_5Sb, C_6Sb, $C_{10}Sb$, and $C_{11}Sb$ are 1.27, 1.25, 1.17, 1.03, and 1.01 eV with 6-31G(d), while the HOMO-LUMO gaps are nearly identical with def2-TZVP basis set (1.26, 1.27, 1.16, 1.04, and 0.99 eV, respectively).

Table 7. The selected structural parameters (the C-C bond adjacent to Sb and the C-Sb bond in Å), C-Sb stretching frequencies (in cm^{-1}), and HOMO-LUMO gaps (in eV) for results obtained at the B3LYP/6-31G(d)/SDD and B3LYP/def2-TZVP/SDD level (denoted as normal and italic fonts, respectively) for C_4Sb, C_5Sb, C_6Sb, $C_{10}Sb$, and $C_{11}Sb$.

	C_4Sb	C_5Sb	C_6Sb	$C_{11}Sb$	$C_{12}Sb$
C-C	1.277 *1.267*	1.288 *1.281*	1.277 *1.267*	1.284 *1.275*	1.274 *1.263*
C-Sb	1.941 *1.941*	1.946 *1.941*	1.949 *1.949*	1.949 *1.949*	1.964 *1.966*
C-Sb Stretching frequency	378.3 *384.5*	331.3 *335.2*	291.7 *294.9*	204.8 *204.9*	190.4 *189.6*
HOMO-LUMO gap	1.27 *1.26*	1.25 *1.27*	1.17 *1.16*	1.03 *1.04*	1.01 *0.99*

2.2. Electronic Configuration

The total symmetry of the pure carbon chain is $D_{\infty h}$ The core electron configuration for carbon is $1s^2$, and for antimony, $1s^22s^22p^63s^23p^63d^{10}4s^24p^64d^{10}$. C_nSb has, therefore, $4n + 5$ valence electrons. Based on molecular orbital theory, quantum chemical computations predict the electronic configurations of the linear ground-state C_nSb clusters as:

$$C_nSb \begin{cases} (\text{core})1\sigma^22\sigma^21\pi^43\sigma^1, n = 1 \\ (\text{core})1\sigma^22\sigma^23\sigma^2\cdots(n+2)\sigma^2 \qquad \frac{2n+1}{2}\pi^2, \text{ n is odd} \\ (\text{core})1\sigma^22\sigma^23\sigma^2\cdots(n+2)\sigma^2 n\pi^2\pi^1, \text{ n is even} \end{cases}$$

Table 8 lists the valence orbital configuration of C_nSb (n = 1–16) clusters. C_nSb possesses $(2n + 1)$ valence π-electrons and $(2n + 4)$ valence σ-electrons. The $(2n + 4)$ valence σ-electrons fully occupy the $(n + 2)$ σ-orbitals. C_nSb has a $\cdots \pi^1$ electronic configuration, $^2\Pi$ state for *n*-even members and a $\cdots \pi^3$ electronic configuration, $^2\Pi$ state for *n*-odd members. C_nSb^+ anions contain $2n$ valence π-electrons; even for *n*, these $2n$ π-electrons should fully populate *n* and doubly degenerate π-orbitals, resulting in a $\ldots \pi^4$ electronic configuration and a $^1\Sigma^+$

state while for odd n, the highest occupied molecular orbital (HOMO) with π-symmetry is half-filled with two electrons, resulting in a $\cdots \pi^2$ electronic configuration and a $^3\Sigma^-$ state. For C_nSb^- anions, the situation is just the opposite. Two more π-electrons result in fully filled π-orbitals in n-odd C_nSb^- clusters and a half-filled π-orbital in n-odd C_nSb^- clusters.

Table 8. Valence orbital configuration of C_nSb.

n	orbital configuration
1	(core) $1\sigma^2 2\sigma^2 1\pi^4 3\sigma^1$
2	(core)$1\sigma^2 2\sigma^2 3\sigma^2 4\sigma^2 1\pi^4 2\pi^1$
3	(core)$1\sigma^2 2\sigma^2 3\sigma^2 4\sigma^2 1\pi^4 5\sigma^2 2\pi^3$
4	(core)$1\sigma^2 2\sigma^2 3\sigma^2 4\sigma^2 5\sigma^2 1\pi^4 2\pi^4 6\sigma^2 3\pi^1$
5	(core)$1\sigma^2 2\sigma^2 3\sigma^2 4\sigma^2 5\sigma^2 1\pi^4 6\sigma^2 2\pi^4 7\sigma^2 3\pi^3$
6	(core)$1\sigma^2 2\sigma^2 3\sigma^2 4\sigma^2 5\sigma^2 6\sigma^2 1\pi^4 7\sigma^2 2\pi^4 3\pi^4 8\sigma^2 4\pi^1$
7	(core)$1\sigma^2 2\sigma^2 3\sigma^2 4\sigma^2 5\sigma^2 6\sigma^2 7\sigma^2 1\pi^4 8\sigma^2 2\pi^4 3\pi^4 9\sigma^2 4\pi^3$
8	(core)$1\sigma^2 2\sigma^2 3\sigma^2 4\sigma^2 5\sigma^2 6\sigma^2 7\sigma^2 8\sigma^2 1\pi^4 9\sigma^2 2\pi^4 3\pi^4 4\pi^4 10\sigma^2 5\pi^1$
9	(core)$1\sigma^2 2\sigma^2 3\sigma^2 4\sigma^2 5\sigma^2 6\sigma^2 7\sigma^2 8\sigma^2 9\sigma^2 1\pi^4 2\pi^4 10\sigma^2 3\pi^4 4\pi^4 11\sigma^2 5\pi^3$
10	(core)$1\sigma^2 2\sigma^2 3\sigma^2 4\sigma^2 5\sigma^2 6\sigma^2 7\sigma^2 8\sigma^2 9\sigma^2 10\sigma^2 1\pi^4 2\pi^4 11\sigma^2 3\pi^4 4\pi^4 5\pi^4 12\sigma^2 6\pi^1$
11	(core)$1\sigma^2 2\sigma^2 3\sigma^2 4\sigma^2 5\sigma^2 6\sigma^2 7\sigma^2 8\sigma^2 9\sigma^2 10\sigma^2 11\sigma^2 1\pi^4 2\pi^4 12\sigma^2 3\pi^4 4\pi^4 5\pi^4 13\sigma^2 6\pi^3$
12	(core)$1\sigma^2 2\sigma^2 3\sigma^2 4\sigma^2 5\sigma^2 6\sigma^2 7\sigma^2 8\sigma^2 9\sigma^2 10\sigma^2 11\sigma^2 12\sigma^2 1\pi^4 2\pi^4 13\sigma^2 3\pi^4 4\pi^4 5\pi^4 6\pi^4 14\sigma^2 7\pi^1$
13	(core)$1\sigma^2 2\sigma^2 3\sigma^2 4\sigma^2 5\sigma^2 6\sigma^2 7\sigma^2 8\sigma^2 9\sigma^2 10\sigma^2 11\sigma^2 12\sigma^2 13\sigma^2 1\pi^4 2\pi^4 14\sigma^2 3\pi^4 4\pi^4 5\pi^4 6\pi^4 15\sigma^2 7\pi^3$
14	(core)$1\sigma^2 2\sigma^2 3\sigma^2 4\sigma^2 5\sigma^2 6\sigma^2 7\sigma^2 8\sigma^2 9\sigma^2 10\sigma^2 11\sigma^2 12\sigma^2 13\sigma^2 14\sigma^2 1\pi^4 2\pi^4 3\pi^4 15\sigma^2 4\pi^4 5\pi^4 6\pi^4 7\pi^4 16\sigma^2 8\pi^1$
15	(core)$1\sigma^2 2\sigma^2 3\sigma^2 4\sigma^2 5\sigma^2 6\sigma^2 7\sigma^2 8\sigma^2 9\sigma^2 10\sigma^2 11\sigma^2 12\sigma^2 13\sigma^2 14\sigma^2 15\sigma^2 1\pi^4 2\pi^4 3\pi^4 16\sigma^2 4\pi^4 5\pi^4 6\pi^4 7\pi^4 17\sigma^2 8\pi^3$
16	(core)$1\sigma^2 2\sigma^2 3\sigma^2 4\sigma^2 5\sigma^2 6\sigma^2 7\sigma^2 8\sigma^2 9\sigma^2 10\sigma^2 11\sigma^2 12\sigma^2 13\sigma^2 14\sigma^2 15\sigma^2 16\sigma^2 1\pi^4 2\pi^4 3\pi^4 17\sigma^2 4\pi^4 5\pi^4 6\pi^4 7\pi^4 8\pi^4 18\sigma^2 9\pi^1$

The frontier molecular orbitals are depicted in Figure 7 with an isovalue of 0.02. Except for the CSb molecule, the LUMO of the other carbon chain clusters exhibits the same orbital shape as HOMO. The smallest CSb shows the σ-character of HOMO, while all the other C_nSb chain clusters show π-character HOMO with overlapping p orbitals shoulder to shoulder. For HOMO, the p orbital of the terminal carbon of the even-numbered carbon cluster always presents a different sign from the p orbital of antimony. While the p orbital of the terminal carbon of odd-numbered carbon cluster exhibits the same sign with a p orbital of antimony, it can form π bonding orbital with antimony. Therefore, the C-Sb bond of C_nSb with even-numbered carbon should be weaker than the C-Sb bond of $C_{n\pm1}Sb$ with odd-numbered carbon. This result agrees well with the Wiberg bond index analysis that the C-Sb WBI of C_nSb with an even n tends to be smaller than the C-Sb WBI of C_nSb with odd n.
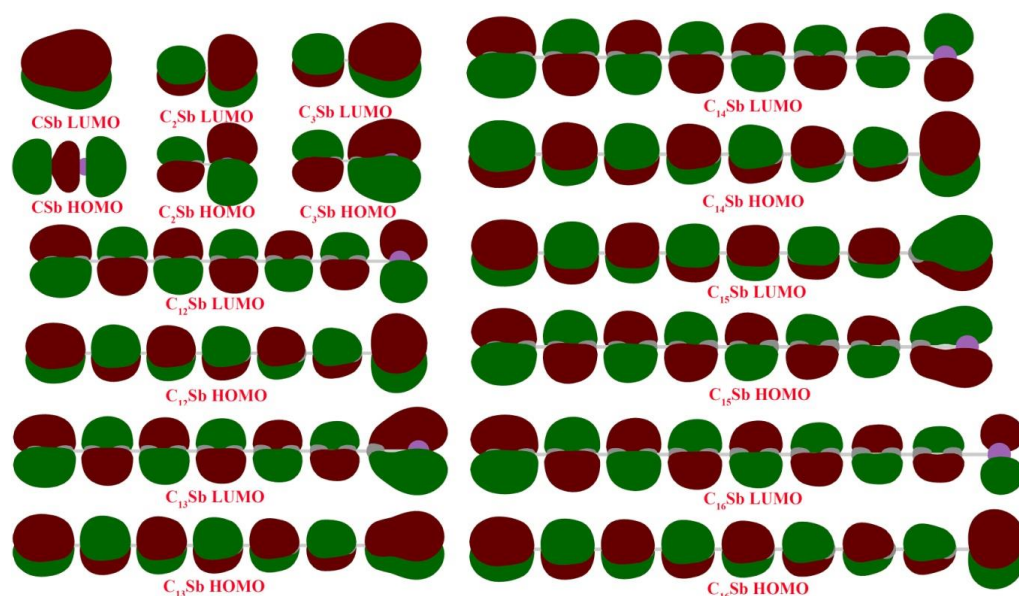

Figure 7. Highest occupied molecular orbitals (HOMO) and lowest unoccupied molecular orbitals (LUMO) for carbon chain clusters. The surface isovalue for molecular orbitals is 0.02.

2.3. Electronic Properties

As is known, the ion signal intensity in a mass spectrum is related to the electron affinity (EA) or ionization energies (IE, also called electron detachment energy) of the molecule. Thus, adiabatic ionization energies, defined as the energy required to remove an electron from the neutral clusters with a geometric change, are important parameters to understand the relative stability of the antimony-doped clusters with different sizes. Usually, there are three types of IE: Koopmans IE, vertical IE, and adiabatic IE. Koopmans IE is the HOMO energy, vertical IE is the energy difference between the neutral and ionic clusters at the neutral equilibrium geometry, and adiabatic IE is the energy difference between the neutral and ionic clusters at their respective equilibrium geometry (i.e., IE = E(optimized cation) − E(optimized neutral)). In this work, the adiabatic IE of C_nSb and C_n clusters for their optimized structures were calculated and shown in Table 4 and Figure 8. As a whole, the ionization energies decrease with the size of the clusters, suggesting that larger C_nSb chains become less stable, e.g., when exposed to a strong electrical field or high temperature. As shown in Figure 8, the adiabatic IE of pure carbon chains C_n has a stair-step shape ($n \geq 6$), whereas C_nSb chains take the shape of a flat curve with a smaller gradient than pure carbon chains. The adiabatic IEs of the even and odd pure carbon chains ($n \geq 6$) follow some nonlinear relationship; the IEs of carbon chains are larger than that of corresponding C_nSb, but the energy difference between them (IE_{C_n}-IE_{C_nSb}) decreases when n increases. The electron affinity (EA) of C_nSb is defined as the energy released when an electron is attached to neutral C_nSb:

EA = *E*(optimized neutral) – *E*(optimized anion).
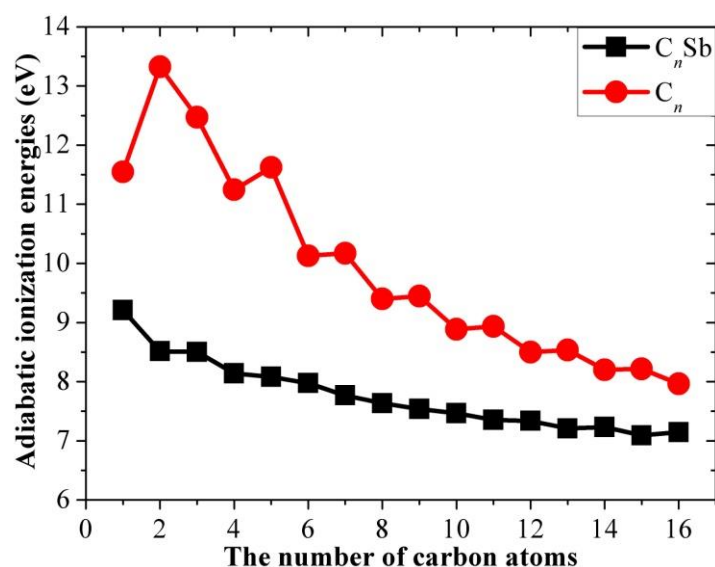
Figure 8. Adiabatic ionization energies of neutral C_nSb and pure carbon clusters C_n as a function of the number of carbons.

This property is also related to the stability of the molecule in the TOF experiment and molecule. A higher EA means that more energy is released when an electron is added to a neutral molecule, and the generation of the corresponding anion is more readily performed. The calculated adiabatic EA data are presented in Table 4. In Figure 9, we compared the adiabatic EAs of C_nSb with that of pure carbon chains: the EAs of carbon chains have a clear alternation parity effect, the EAs of carbon chains with an even n are larger than the EAs of adjacent n-odd members but carbon chains doped with the antimony atom do not exhibit a parity effect. The computed EAs of the even and odd carbon chains followed a non-linear relationship with the number of carbons, respectively. The energy difference between EA_{C_n} and EA_{C_nSb} was much smaller than (IE_{C_n} - IE_{C_nSb}), except when $n = 1$, and EA_{C_n} was slightly larger than EA_{C_nSb} when $n \geq 10$.
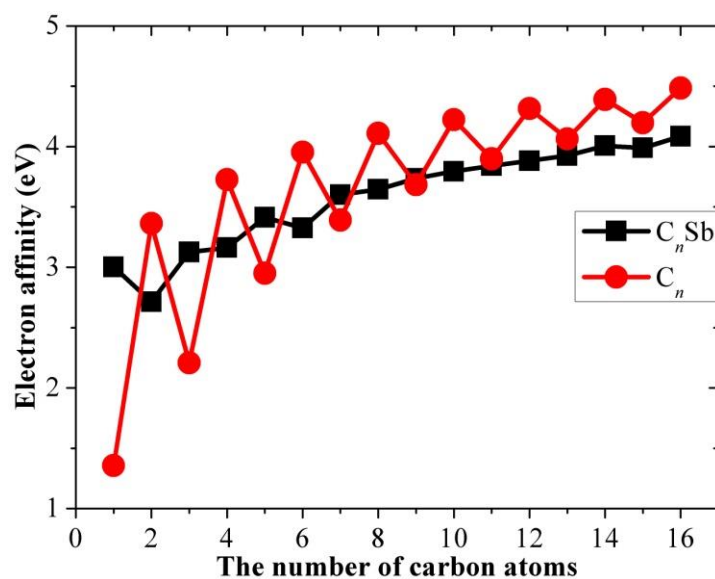
Figure 9. Adiabatic electron affinities of neutral C_nSb and pure carbon clusters C_n as a function of the number of carbons.

All the antimony atoms of C_nSb show positive charges, indicating that antimony denotes electrons to the carbon cluster. The antimony of CSb carries the least positive charge of 0.33 |e|, while the antimony of C_2Sb carries the most positive charge of 0.52 |e|. Antimony atoms of larger C_nSb ($n > 3$) chain clusters show positive charges 0.43, 0.44, 0.49, 0.44, 0.48, 0.44, 0.46, 0.44, 0.46, 0.44, 0.45, 0.44, and 0.44 |e|, respectively. Thus, the carbon chain with an even-number of carbon atoms tends to exhibit higher antimony charges. The carbon atom nearest to antimony showed a negative charge due to the electron donation of antimony (Table 9). Without doping antimony, the two anomeric carbons at the right and the left end of the pure carbon chain show an identical charge value. With the antimony doping, the anomeric carbon shows significant charge differences (Table 9 and Figure 10). The charge differences between anomeric carbon atoms are calculated to be 0.43, 0.31, 0.51, 0.53, 0.62, 0.6, 0.65, 0.63, 0.66, 0.64, 0.67, 0.65, 0.67, 0.65, and 0.67 |e| for C_nSb (n = 2–16). This result suggests that the doping of antimony definitely changed the charge population of the carbon cluster.

Table 9. The charge population and charge difference ($|\Delta C|$) of terminal carbon atoms which are adjacent antimony (C1) and far away from antimony (C2).

Species	C1	C2	$|\Delta C|$	Species	C1	C2	$|\Delta C|$
C_1Sb	−0.33			C_9Sb	−0.76	−0.14	0.63
C_2Sb	−0.47	−0.05	0.42	$C_{10}Sb$	−0.80	−0.14	0.66
C_3Sb	−0.45	−0.14	0.31	$C_{11}Sb$	−0.77	−0.13	0.64
C_4Sb	−0.73	−0.22	0.51	$C_{12}Sb$	−0.80	−0.13	0.67
C_5Sb	−0.72	−0.19	0.53	$C_{13}Sb$	−0.77	−0.13	0.65
C_6Sb	−0.80	−0.18	0.62	$C_{14}Sb$	−0.80	−0.13	0.67
C_7Sb	−0.75	−0.15	0.60	$C_{15}Sb$	−0.78	−0.13	0.65
C_8Sb	−0.80	−0.15	0.65	$C_{16}Sb$	−0.80	−0.13	0.67
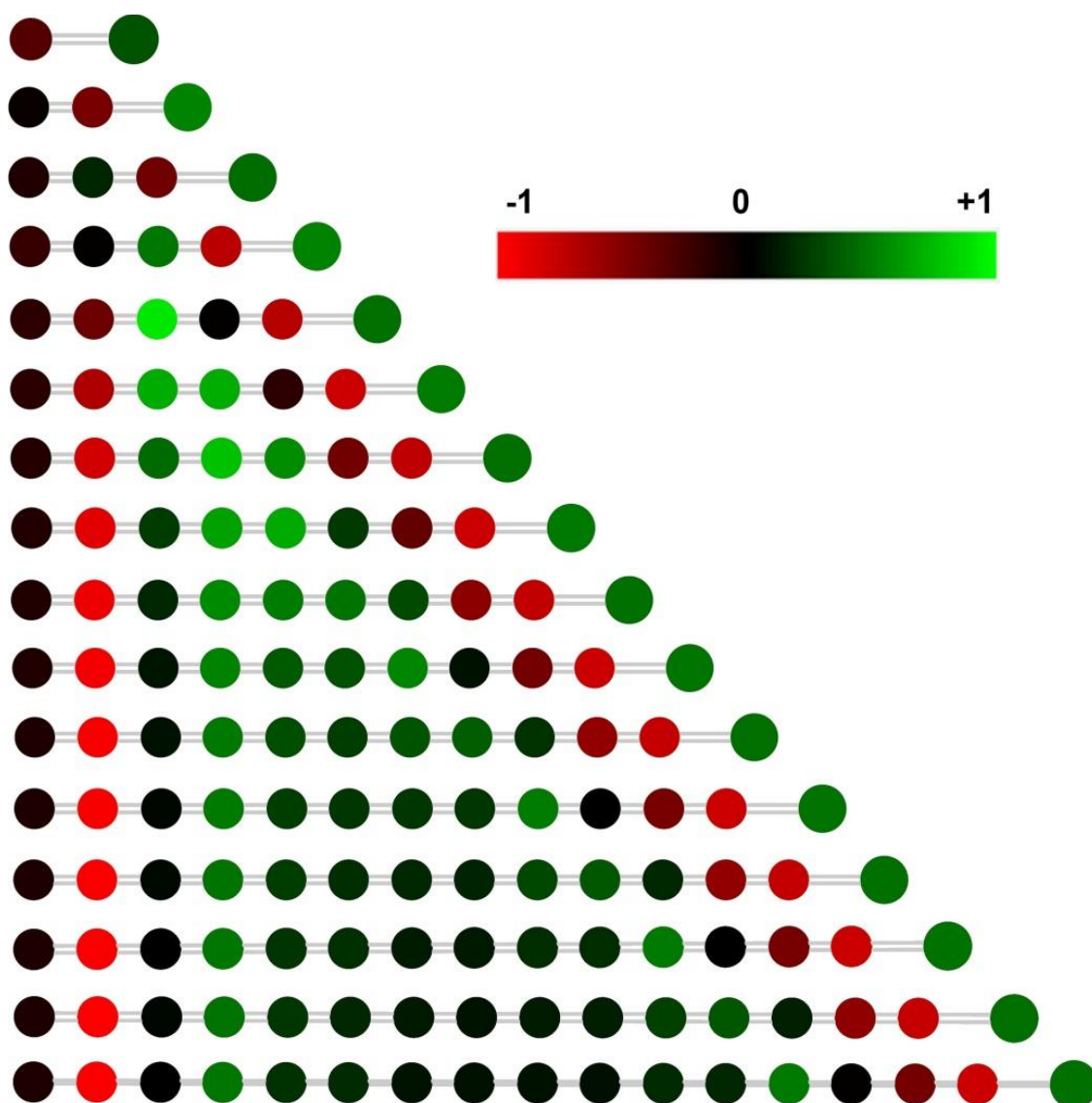
Figure 10. The NPA (natural population analysis) charge distribution for C$_n$Sb chain clusters. The color range is depicted from −1 to 1. The small balls and the large balls in the right end indicate carbon and antimony atoms, respectively.

The Wiberg bond indices of C$_n$Sb are listed in Figure 11. The C-Sb bond is a double bond with WBI between 1.41 and 2.13, which is obviously stronger for a carbon chain cluster with odd-number carbon atoms (compared with neighboring carbon chain clusters with even-number carbon atoms). The WBI of all C-C bonds was determined to be between 1.63 and 2.01, indicating the cumulene character of the carbon chain. Generally, the alteration of WBI and, in particular, the carbon chain cluster is consistent with the bond length alteration. However, the shorter C-C distance did not indicate a larger WBI. For example, the largest WBI for C$_n$Sb ($n > 1$) was calculated to be the terminal C-C bond index, while this terminal C-C bond was not the shortest C-C bond. Therefore, rather than relying on the empirical comparison of bond distance, the WBI is a meaningful quantitative indicator for predicting the bonding strength in the carbon chain.

Figure 11. Computed Wiberg bond indices (WBI) for C_nSb.

2.4. Incremental Energies, Fragmental Energies, and Binding Sites

The relative stability of clusters can be also analyzed in terms of the energy differences between the neighboring size of the clusters, which is correlated with the "magic number" in cluster science [36]. Energy differences between C_nSb and $C_{n-1}Sb$, C_nSb^+ and $C_{n-1}Sb^+$, C_nSb^- and $C_{n-1}Sb^-$ (differential energies ΔE_n, defined as $\Delta E_n = E_n - E_{n-1}$) are listed in Tables 5–7, respectively. For the clusters with different sizes, the concept of the incremental binding energy, labeled as ΔE^I, was introduced to compare their relative stabilities. As suggested by Pascoli and Lavendy [37,38], ΔE^I is just the reaction energy of the following processes:

$C_nSb \rightarrow C_{n-1}Sb + C$ (DN1)
$C_nSb^+ \rightarrow C_{n-1}Sb^+ + C$ (DC1)
$C_nSb^- \rightarrow C_{n-1}Sb^- + C$ (DA1)
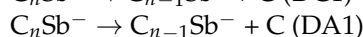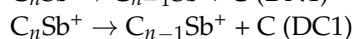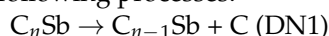
They can be computed as the consecutive binding energy (BE, atomization energy, listed in Tables 5–7) differences between the adjacent clusters,

$\Delta E^I(C_nSb/C_nSb^+/C_nSb^-) = BE(C_nSb/C_nSb^+/C_nSb^-) - BE(C_{n-1}Sb/C_{n-1}Sb^+/C_{n-1}Sb^-)$

where BE can be defined as the energy difference between a molecule and its component atoms:

$BE(C_nSb/C_nSb^+/C_nSb^-) = nE(C) + E(Sb) - E(C_nSb/C_nSb^+/C_nSb^-)$

The results for the incremental binding energy as a function of the number of carbon atoms for the different open-chain $C_nSb/C_nSb^+/C_nSb^-$ clusters and pure carbon chains are shown in Figures 12–14. It can be observed that there is an even-odd alternation for the open chain C_nSb and C_nSb^+ ($n = 1$–10, when $n > 10$, the parity effect is less obvious and n-odd members of C_nSb^+ are slightly larger), with even species being comparatively more stable than odd ones; the parity variation tendency of neutral C_nSb is opposite to that of pure C_n (i.e., n-even carbon chains are less stable than adjacent n-odd ones) and the

variation amplitude is much smaller than pure C_n. The difference in ΔE^{I} between the even and odd species of both C_nSb and pure C_n chains diminishes with the increase in carbon atoms; different from C_n^- anions, the ΔE^{I} for C_nSb$^-$ anions did not exhibit a parity effect. However, these patterns of ΔE^{I} for C_nSb$^+$ and C_nSb$^-$ cannot be simply explained by the "valence π-electron number" rule.
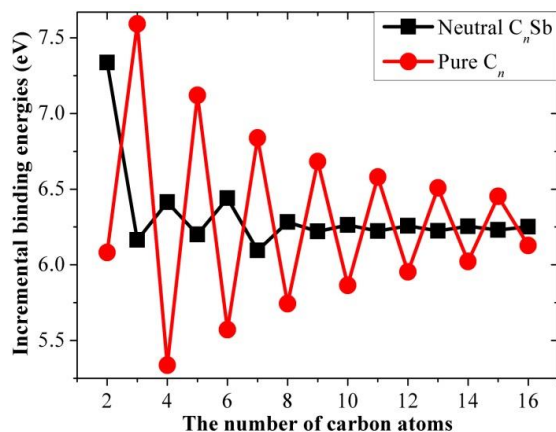
Figure 12. Increment binding energies of C_nSb and pure C_n chains as a function of the number of carbon atoms.
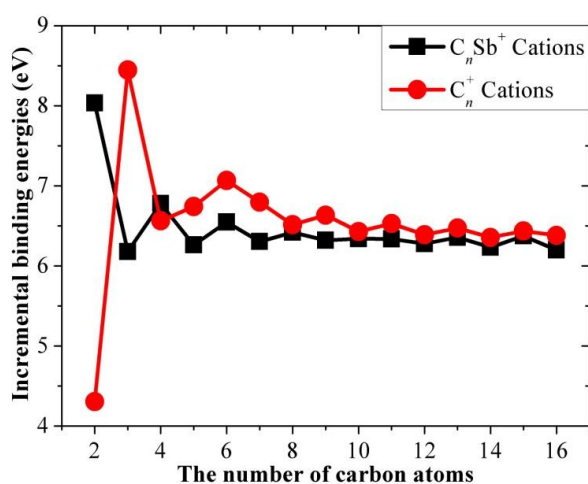
Figure 13. Incremental binding energies of C_nSb$^+$ cations and pure C_n cations as a function of the number of carbon atoms.
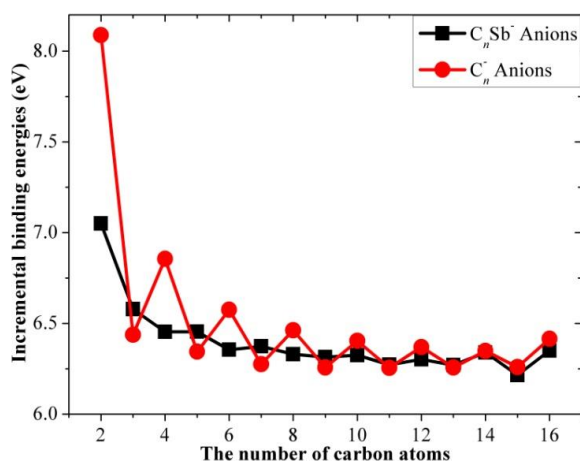
Figure 14. Incremental binding energies of C_nSb$^-$ anions and pure C_n^- anions.

The fragmentation energies accompanying channels DN1, DC1, and DA1, i.e., $\triangle E^{\mathrm{I}}$, have been discussed. In addition, the fragmentation energies for many other dissociation reactions are calculated and exhibited in Figures 15–17, including the following seven channels for neutral C_nSb clusters:
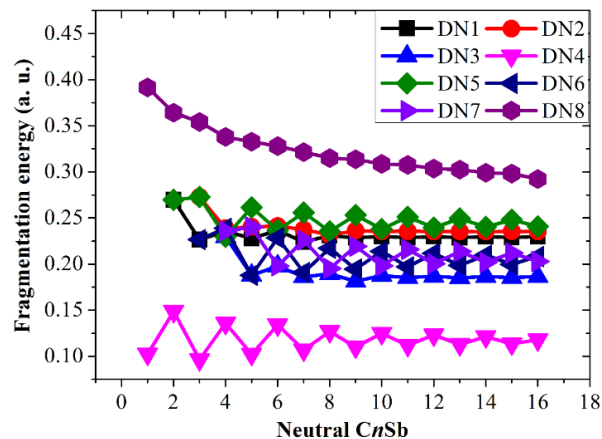
Figure 15. Fragmentation energies of neutral C_nSb clusters. DNx corresponds to different dissociation channels, as shown in the text.
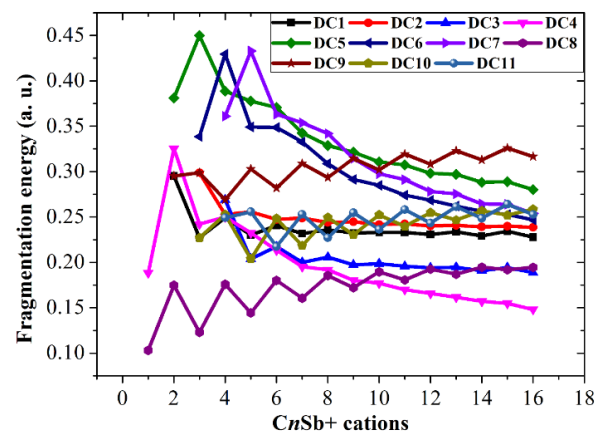
Figure 16. Fragmentation energies of C_nSb$^+$ cations. DC*x* corresponds to different dissociation channels, as shown in the text.
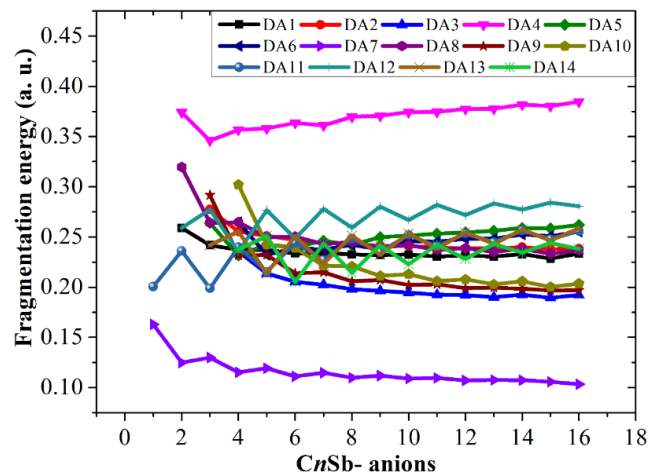
Figure 17. Fragmentation energies of C_nSb$^-$ anions. DA*x* corresponds to different dissociation channels, as shown in the text.

$C_nSb \rightarrow C_{n-2}Sb + C_2 (DN2)$

$C_nSb \rightarrow C_{n-3}Sb + C_3 (DN3)$

$C_nSb \rightarrow C_n + Sb (DN4)$

$C_nSb \rightarrow C_{n-1} + CSb (DN5)$

$C_nSb \rightarrow C_{n-2} + C_2Sb (DN6)$

$C_nSb \rightarrow C_{n-3} + C_3Sb (DN7)$

$C_nSb \rightarrow C_n^- + Sb^+ (DN8)$
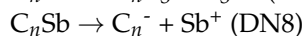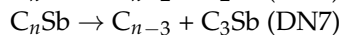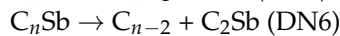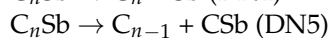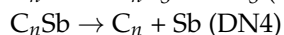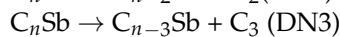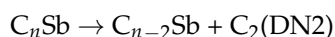
The following ten channels for cationic C_nSb^+ cations:

$C_nSb^+ \rightarrow C_{n-2}Sb^+ + C_2 (DC2)$

$C_nSb^+ \rightarrow C_{n-3}Sb^+ + C_3 (DC3)$

$C_nSb^+ \rightarrow C_n^+ + Sb (DC4)$

$C_nSb^+ \rightarrow C_{n-1}^+ + CSb (DC5)$

$C_nSb^+ \rightarrow C_{n-2}^+ + C_2Sb (DC6)$

$C_nSb^+ \rightarrow C_{n-3}^+ + C_3Sb (DC7)$

$C_nSb^+ \rightarrow C_n + Sb^+ (DC8)$

$C_nSb^+ \rightarrow C_{n-1} + CSb^+ (DC9)$

$C_nSb^+ \rightarrow C_{n-2} + C_2Sb^+ (DC10)$

$C_nSb^+ \rightarrow C_{n-3} + C_3Sb^+ (DC11)$
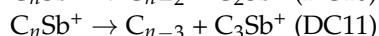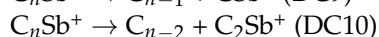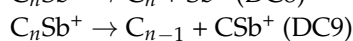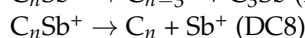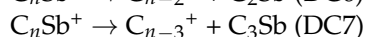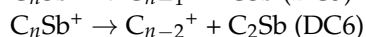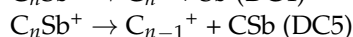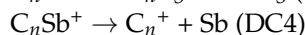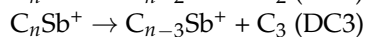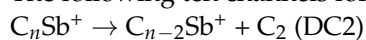
and the following thirteen channels for anionic C_nSb^- anions:

$C_nSb^- \rightarrow C_{n-2}Sb^- + C_2 (DA2)$

$C_nSb^- \rightarrow C_{n-3}Sb^- + C_3 (DA3)$

$C_nSb^- \rightarrow C_{n-1}Sb + C^- (DA4)$

$C_nSb^- \rightarrow C_{n-2}Sb + C_2^- (DA5)$

$C_nSb^- \rightarrow C_{n-3}Sb + C_3^- (DA6)$

$C_nSb^- \rightarrow C_n^- + Sb (DA7)$

$C_nSb^- \rightarrow C_{n-1}^- + CSb (DA8)$

$C_nSb^- \rightarrow C_{n-2}^- + C_2Sb (DA9)$

$C_nSb^- \rightarrow C_{n-3}^- + C_3Sb (DA10)$

$C_nSb^- \rightarrow C_n + Sb^- (DA11)$

$C_nSb^- \rightarrow C_{n-1} + CSb^- (DA12)$

$C_nSb^- \rightarrow C_{n-2} + C_2Sb^- (DA13)$

$C_nSb^- \rightarrow C_{n-3} + C_3Sb^- (DA14)$
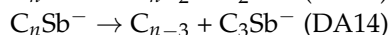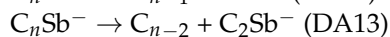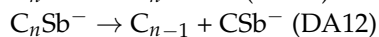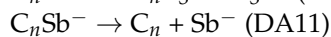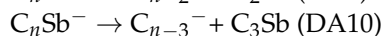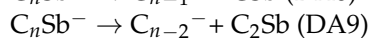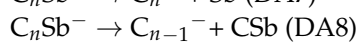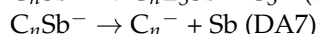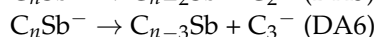
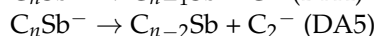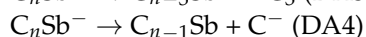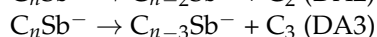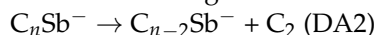These channels can be divided into four types: (1) losing neutral small carbon particles such as C, C_2, or C_3; (2) losing neutral antimony-contained small fragments such as Sb, CSb, C_2Sb, or C_3Sb; (3) losing ionic defects, such as Sb^+/Sb^-, CSb^+/CSb^-, C_2Sb^+/C_2Sb^-, or C_3Sb^+/C_3Sb^- fragments (for C_nSb^+/C_nSb^-); and (4) losing anionic carbons, such as C^-, C_2^-, and C_3^- fragments (only for C_nSb^-). Comparing the fragmentation energies can help us to find some dominant channels for each kind of cluster in the discussion.

The fragmentation energies of channels DN1, DC1, and DA1 are also included for comparison. It is clear that losing an antimony atom is the dominant channel for neutral C_nSb (channel DN4). For small C_nSb^+ cations ($n = 1–9$), the most favorable fragmentation channel is the loss of the Sb^+ ion (channel DC8). However, when $n \geq 10$, losing an antimony atom (DC4) becomes the dominant channel. The most favorable dissociation pathway for CSb^- and C_nSb^- ($n = 2–16$) is the loss of the Sb^- ion and the loss of the antimony atom, respectively. The most favorable dissociation channels for $C_nSb/C_nSb^+/C_nSb^-$ are illustrated in Figure 18, from which we can draw some conclusions: the fragmentation energies for DN4 exhibit a parity effect, i.e., the even C_nSb clusters are more stable while the odd C_nSb clusters are easy to dissociate; the fragmentation energies for DC8 ($n = 1–9$) also showed an alternation effect with the same alternation trend as DN4. the fragmentation energies for DC4 did not show fluctuation or a decrease monotonically as the n number rose; when n > 4 C_nSb^+, is more stable than C_nSb^- anions and neutral C_nSb. The subtle alternation for DA7 exists when $n \leq 10$; when $n > 10$, the C_nSb^- anion is in its least stable form compared with C_nSb and C_nSb^+.
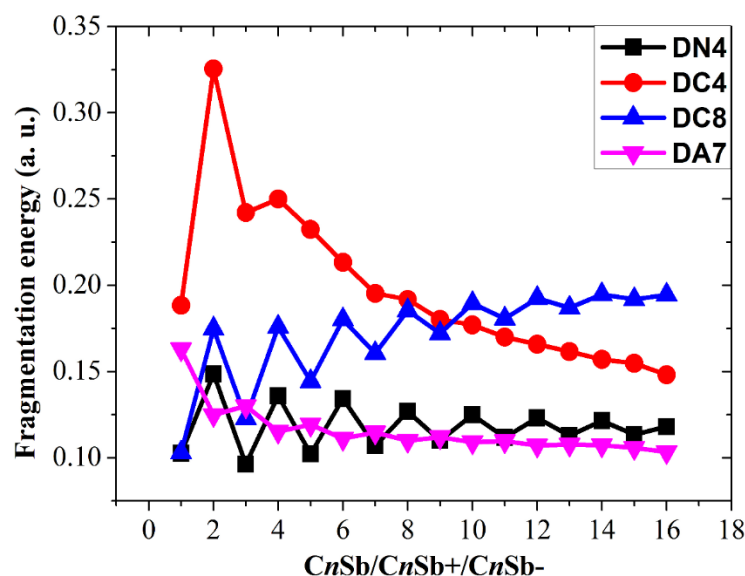
Figure 18. The most favorable dissociation channels for C_nSb/ C_nSb^+ / C_nSb^-.

For carbon chain clusters, the most favorable binding site of atomic antimony is the terminal carbon of the carbon cluster because the terminal carbon with a large spin density bonds in an unsaturated way. We have constructed initial structures with antimony binding on nonterminal carbon and found that the optimization of these structures often encounters a convergence problem or loop back to the linear structure with antimony binding to the terminal carbon. For the structures which encounter convergence problems or converge to geometry with antimony binding on nonterminal carbon, we further optimized them and obtained the local minima (Figure 19). For antimony binding on C_2, the 2a nonlinear structure showed a C-C distance of 1.315 Å, longer than the linear structure. The results indicate that the construction of the nonlinear shape C_nSb can further activate the C-C bond. Nonlinear C_3Sb and C_4Sb show C_{2V} symmetric structures. The C-C bonds of C_3Sb are all 1.335 Å, while the C-C bond adjacent to antimony shows a substantially longer distance of 1.380 Å. Nonlinear C_5Sb with antimony binding on the second or third carbon does not exhibit bond length alteration. Nonlinear C_6Sb and C_7Sb with antimony binding on the third carbon or binding on the bridge site between the third and fourth carbon do not exhibit bond length alteration effects. The C-C bond distances adjacent to antimony are calculated to be 1.346 and 1.360 Å for 5a and 5b, respectively, which are much longer than 1.288 Å for linear C_5Sb. The C-C bond distances adjacent to the antimony of 6a and 6b are calculated to be 1.355 and 1.440 Å, which is much longer than 1.277 Å for the linear carbon chain C_6Sb. The bond length alteration does not exist for nonlinear C_7Sb. The antimony binding on the second or third carbon of C_7 leads to the reconstruction and formation of the linear carbon chain. The bond length alteration effect exists in unstable nonlinear C_8Sb (8c) with s high RBE of 3.93 eV. Structures 8a and 8b do not show the bond length alteration effect.

For the low energy minia of nonlinear C_2Sb to C_8Sb, the adiabatic ionization energies were calculated to be 8.54, 7.19, 9.09, 6.14, 4.82, 8.06, and 8.26 eV, respectively, indicating that the nonlinear C_5Sb and C_6Sb could be more easily ionized. Comparatively, the linear carbon chains C_nSb show more constant adiabatic ionization energy with the increase in the carbon number. The relative binding energies of nonlinear C_2Sb to C_8Sb with antimony binding on the sides of carbon clusters (relative to the binding energy of the linear chain cluster) are calculated to be 0.4, 1.23, 1.53, 1.8, 2.86, 2.54, and 2.82 eV, respectively. The results indicate that the relative binding energy is significantly large except for the much smaller carbon cluster C_2Sb. Quantitatively, the binding energy of nonlinear C_2Sb to C_8Sb with antimony binding on the sides of carbon clusters were calculated to be -3.33, -3.24, -1.85, -2.64, -0.34, -1.52, and -0.28 eV, respectively. Antimony is a metallic element

exhibiting low electron affinity. If the antimony atom is changed to nitrogen with strong electronegativity, we can test the structural geometry, adiabatic ionization energy, and natural charge population of C_6N and C_7N. The bond length alteration effect of C_6N and C_7N is much different from that in C_6Sb and C_7Sb. The bond length difference between the adjacent C-C bonds is larger than that in the antimony-doped carbon chain cluster. The C-C bond adjacent to nitrogen is substantially longer than that adjacent to antimony. The adiabatic ionization energies of C_6N and C_7N were calculated to be 8.82 and 9.17 eV, which are larger than the C_6Sb and C_7Sb, indicating the higher stability of the nitrogen-doped carbon chain. Different from the charging state of antimony, the natural charge population analysis of C_6N and C_7N indicates that nitrogen atoms are both negatively charged with -0.42 |e|.
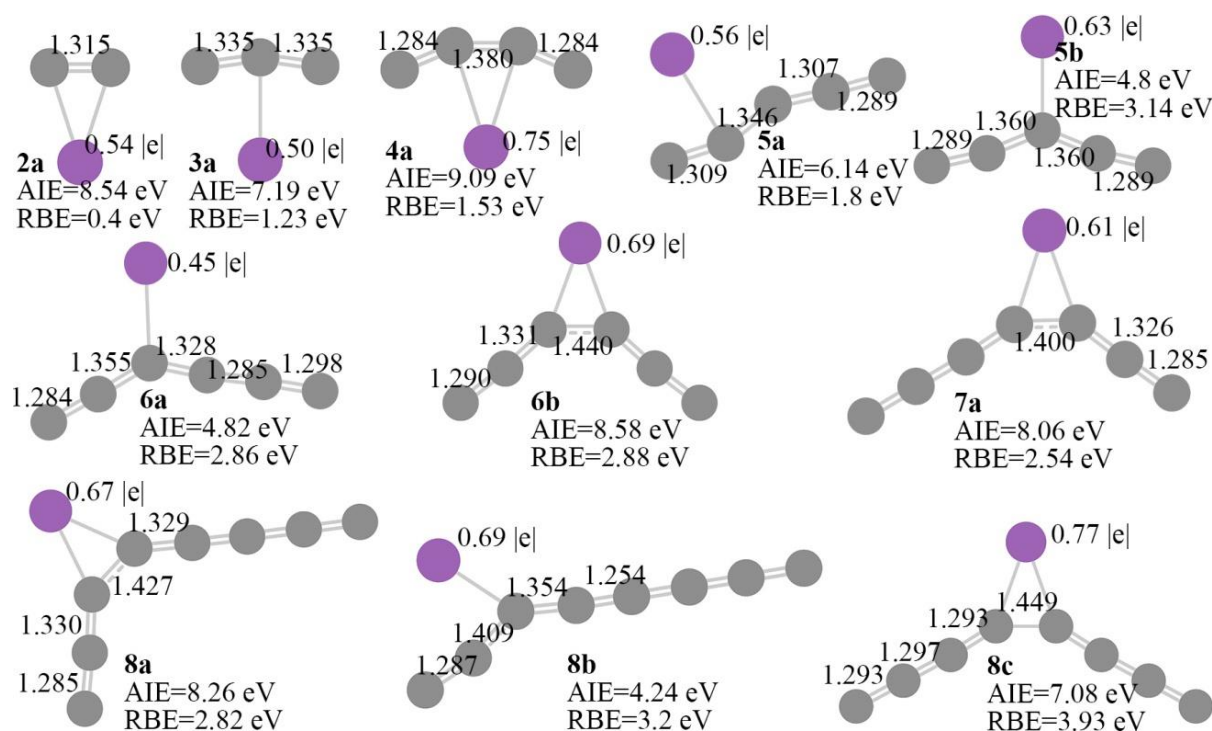

Figure 19. Structural geometry, adiabatic ionization energy (AIE), relative binding energy (RBE), and charge population influenced by binding site of antimony atom. Relative binding energy is calculated by equation: $RBE = E_b(nt) - E_b(t)$, where $E_b(nt)$ and $E_b(t)$ stand for structure with antimony binding on nonterminal carbon and linear structure with antimony binding on terminal carbon, respectively. Notations na, nb, and nc represent the structures with *n* carbon atoms.

3. Computational Methods

To explore the structure and energetics in the linear antimony-doped carbon clusters, full geometry optimizations were performed using density-functional theory methods implemented in the Gaussian 03 program [39]. The Molecular mechanic's algorithm is frequently employed to investigate very large carbon-based materials because of the efficiency in predicting the binding and delivery mechanism. Density-functional calculations are verified to be effective and have an accurate strategy to reveal the geometric structures [40,41] and electronic properties of various nanomaterials [42–45]. The B3LYP exchange-correlation function consists of Fock's exact exchange and Beck's three-parameter nonlocal exchange function, along with the nonlocal correlation function developed by Lee et al. [46]. B3LYP was chosen here because the previous research suggests that hybrid-functional is reliable and highly efficient for molecules and clusters [47,48], while the post-HF Ab initio method is accurate but time-consuming [49,50]. A medium-size basis set 6-31G(d) was used for a carbon atom, and the Stuttgart/Bonn relativistic effective core potential (SDD) basis set

was used for antimony. The geometries and relative energies of heteroatom-doped carbon clusters obtained with the B3LYP method were very close to those with the coupled cluster single and double (triple) (CCSD(T)) and QCISD(T) method [51,52]. Vibrational frequencies were computed at the same level using a harmonic approximation to assess the nature of the optimized structures. Zero-point energies (ZPE) were evaluated as well using the same methodology. The optimized structures were then used for single-point calculations at the B3LYP/6-311++G(3df,3pd) level. In the computation, bond lengths of the magnetic neutral CnSb, CnSb$^+$ cations, and CnSb$^-$ anions (n = 1–16) clusters have been optimized through the use of B3LYP methods with a 6-31G(d) basis set. Subsequently, the corresponding harmonic vibrational frequencies are evaluated at the same level. To further verify the reliability of the optimized geometries, we have carefully checked every computation step that might cause possible numerical calculation errors. We have adopted the default convergence criteria for self-consistent-field (SCF) calculation, i.e., 10^{-8} for the root mean square density and 10^{-6} for the maximum density, and for geometry optimization, 0.00030 This includes the Hartree/Bohr radius for the root mean square force and 0.00045 Hartree/Bohr radius for the maximum force. In addition, the convergence criteria for the energy change in the final step of geometry optimization was set to be 10^{-7} Hartree.

4. Conclusions

The linear carbon chain cluster with different lengths and doping atoms is a special allotrope type of carbon material different from graphite, diamond, graphene, carbon nanotubes, and fullerenes. We have conducted a systematic DFT study on linear $C_nSb/C_nSb^+/C_nSb^-$ clusters with sizes of n = 1–16 and compared these with pure C_n clusters. C-C bond lengths of the linear neutral C_nSb, C_nSb^+ cations and C_nSb^- anions are within 0.1255−0.1336 nm, which is typical of cumulene structures with moderately strong double bonds. However, the alternation in C-C distances suggests that there is a substantial contribution of polyacetylenic valence-bond structures with an alternating triple and single C-C bond. The C-C BLA of neutral CnSb is obvious for n-even clusters, and for n-odd clusters, the BLA tends to be irregular in the vicinity of Sb. We can deduct from C-C BLA and C-Sb BLA that the antimony atom of n-odd C_nSb^- anions and n-even C_nSb^+ (n = 1–10) cations are combined more firmly than adjacent clusters. This is roughly proved to be right by our calculation of their dissociation channels. When comparing the BLA of neutral and charged antimony-doped carbon chains to that of pure carbon chains, it is easy to deduce that through doping the antimony element, the properties of carbon clusters are changed. The adiabatic IE of C_nSb decreased with the rise in the n number, suggesting that larger C_nSb chains become less stable. When comparing the IE of C_nSb with that of pure C_n, we found that the latter had a stair-step pattern ($n \geq 6$), but C_nSb chains took the shape of a flat curve. The IEs of carbon chains are larger than that of corresponding C_nSb, but the energy difference (IE_{Cn}-IE_{CnSb}) decreases with increasing n. Different from pure carbon chains, the adiabatic electron affinity of C_nSb do not exhibit a parity effect. There is an even-odd alternation for $\triangle E^I$ of the open chain C_nSb (n = 1–16) and C_nSb^+ (n = 1–10, when $n > 10$, $\triangle E^I$ of n-odd members of C_nSb^+ are larger), with the n-even species being comparatively more stable than n-odd ones. The $\triangle E^I$ for C_nSb^- anions does not exhibit a parity effect. For carbon chain clusters, the most favorable binding site of atomic antimony is the terminal carbon of the carbon cluster because the terminal carbon with a large spin density bonds in an unsaturated way. The C-Sb bond is a double bond with WBI between 1.41 and 2.13, which is obviously stronger for a carbon chain cluster with odd-number carbon atoms (compared with neighboring carbon chain clusters with even-number carbon atoms). The WBI of all C-C bonds was determined to be between 1.63 and 2.01, indicating the cumulene character of the carbon chain. Generally, the alteration of WBI and, in particular, the carbon chain cluster is consistent with the bond length alteration. However, the shorter C-C distance did not indicate a larger WBI. For example, the largest WBI for C_nSb ($n > 1$) was calculated to be the terminal C-C bond index, while this terminal C-C bond was not the shortest C-C bond. Therefore, rather than relying on the empirical

comparison of bond distance, the WBI is a meaningful quantitative indicator for predicting the bonding strength in the carbon chain. For HOMO, the p orbital of the terminal carbon of the even-numbered carbon cluster always presents a different sign from the p orbital of antimony. While the p orbital of the terminal carbon of odd-numbered carbon cluster exhibits the same sign with a p orbital of antimony, it can form π bonding orbital with antimony. Therefore, the C-Sb bond of C_nSb with even-numbered carbon should be weaker than the C-Sb bond of $C_{n\pm1}Sb$ with odd-numbered carbon. This result agrees well with the Wiberg bond index analysis.

Author Contributions: Conceptualization, Z.S. and M.Y.; methodology, Z.S., X.S., W.W. and H.W.; software, Z.S. and M.Y.; validation, Z.S., M.L. and M.Y.; formal analysis, Z.S.; investigation, Z.S., X.S. and Z.L.; resources, Z.S., Z.L. and H.W.; data curation, Z.S.; writing—original draft preparation, Z.S., M.Y., M.L., X.S. and Z.L.; writing—review and editing, Z.S., H.W. and M.Y.; visualization, Z.S. and M.Y.; supervision, Z.S., H.W., M.Y. and M.L.; project administration, Z.S., M.Y. and H.W.; funding acquisition, Z.S., M.Y., M.L. and H.W. All authors have read and agreed to the published version of the manuscript.

Institutional Review Board Statement: Not applicable.

Informed Consent Statement: Not applicable.

Data Availability Statement: Not applicable.

Conflicts of Interest: The authors declare that they have no known competing financial interests or personal relationships that could have appeared to influence the work reported in this paper.

Sample Availability: Not applicable.

References

1. Leyva-Perez, A. Sub-nanometre metal clusters for catalytic carbon-carbon and carbon-heteroatom cross-coupling reactions. *Dalton T.* **2017**, *46*, 15987–15990. [CrossRef] [PubMed]
2. de Lara-Castells, M.P.; Mitrushchenkov, A.O. Mini Review: Quantum Confinement of Atomic and Molecular Clusters in Carbon Nanotubes. *Front. Chem.* **2021**, *9*, 796890. [CrossRef] [PubMed]
3. Shi, W.; Song, Z.; Wang, J.; Li, Q.; An, Q. Phytic acid conversion film interfacial engineering for stabilizing zinc metal anode. *Chem. Eng. J.* **2022**, *446*, 137295. [CrossRef]
4. Shao, X.; Li, L.; Huang, S.; Song, Z.; Wang, K. First-Principles Calculations of Magnetic Moment Modulation of 3D Transition Metal Atoms Encapsulated in C_{60}/C_{70} Cages on Si(100) Surfaces: Implications for Spintronic Devices. *ACS Appl. Nano Mater.* **2021**, *4*, 12356–12364. [CrossRef]
5. Chen, W.; Huang, J.; He, Z.-C.; Ji, X.; Zhang, Y.-F.; Sun, H.-L.; Wang, K.; Su, Z.-W. Accelerated photocatalytic degradation of tetracycline hydrochloride over $CuAl_2O_4/g$-C_3N_4 p-n heterojunctions under visible light irradiation. *Sep. Purif. Technol.* **2021**, *277*, 119461. [CrossRef]
6. Liu, M.; Yu, T.; Huang, R.; Qi, W.; He, Z.; Su, R. Fabrication of nanohybrids assisted by protein-based materials for catalytic applications. *Catal. Sci. Technol.* **2020**, *10*, 3515–3531. [CrossRef]
7. Pu, D.; Pan, Y. First-principles investigation of solution mechanism of C in TM-Si-C matrix as the potential high-temperature ceramics. *J. Am. Ceram. Soc.* **2022**, *105*, 2858–2868. [CrossRef]
8. Liu, M.; Shan, C.; Chang, H.; Zhang, Z.; Huang, R.; Lee, D.W.; Qi, W.; He, Z.; Su, R. Nano-engineered natural sponge as a recyclable and deformable reactor for ultrafast conversion of pollutants from water. *Chem. Eng. Sci.* **2022**, *247*, 117049. [CrossRef]
9. Tuktarov, A.R.; Khuzin, A.A.; Dzhemilev, U.M. Light-controlled molecular switches based on carbon clusters. Synthesis, properties and application prospects. *Russ. Chem. Rev.* **2017**, *86*, 474–509. [CrossRef]
10. Hadad, C.Z.; Florez, E.; Merino, G.; Cabellos, J.L.; Ferraro, F.; Restrepo, A. Potential Energy Surfaces of WC_6 Clusters in Different Spin States. *J. Phys. Chem. A* **2014**, *118*, 5762–5768. [CrossRef]
11. Stein, T.; Bera, P.P.; Lee, T.J.; Head-Gordon, M. Molecular growth upon ionization of van der Waals clusters containing HCCH and HCN is a pathway to prebiotic molecules. *Phys. Chem. Chem. Phys.* **2020**, *22*, 20337–20348. [CrossRef] [PubMed]

12. Yao, Y.; Xie, S. Structures and Progress of Carbon Clusters. *Prog. Chem.* **2019**, *31*, 50–62.
13. Ticknor, B.W.; Bandyopadhyay, B.; Duncan, M.A. Photodissociation of Noble Metal-Doped Carbon Clusters. *J. Phys. Chem. A* **2008**, *112*, 12355–12366. [CrossRef] [PubMed]
14. Lacovig, P.; Pozzo, M.; Alfe, D.; Vilmercati, P.; Baraldi, A.; Lizzit, S. Growth of dome-shaped carbon nanoislands on Ir(111): The intermediate between carbidic clusters and quasi-free-standing graphene. *Phys. Rev. Lett.* **2009**, *103*, 166101. [CrossRef] [PubMed]
15. Niu, T.C.; Zhou, M.; Zhang, J.L.; Feng, Y.P.; Chen, W. Growth Intermediates for CVD Graphene on Cu(111): Carbon Clusters and Defective Graphene. *J. Am. Chem. Soc.* **2013**, *135*, 8409–8414. [CrossRef] [PubMed]
16. Song, Z.J. First-principle investigation on growth patterns and properties of cobalt-doped lithium nanoclusters. *J. Mol. Model.* **2016**, *22*, 133. [CrossRef]
17. Song, Z.; Zhao, B.; Wang, Q.; Cheng, P. Homolytic cleavage of water on magnesia film promoted by interfacial oxide-metal nanocomposite. *Appl. Surf. Sci.* **2019**, *487*, 1222–1232. [CrossRef]
18. Song, Z.; Shao, X.; Wang, Q.; Ma, C.; Wang, K.; Han, D. Generation of molybdenum hydride species via addition of molecular hydrogen across metal-oxygen bond at monolayer oxide/metal composite interface. *Int. J. Hydrog. Energ.* **2020**, *45*, 2975–2988. [CrossRef]
19. Song, Z.; Fang, S.; Xie, P.; Zhong, A.; Ma, C.; Han, D. Unveiling the interaction profile of cisplatin with gold-supported magnesia film. *Appl. Surf. Sci.* **2021**, *540*, 148365. [CrossRef]
20. Pei, C.-Y.; Li, T.; Zhang, M.; Wang, J.-W.; Chang, L.; Xiong, X.; Chen, W.; Huang, G.-B.; Han, D.-M. Synergistic effects of interface coupling and defect sites in $WO_3/InVO_4$ architectures for highly efficient nitrogen photofixation. *Sep. Purif. Technol.* **2022**, *290*, 120875. [CrossRef]
21. Guo, X.-G.; Zhang, J.-L.; Zhao, Y. Ab initio Characterization of Size Dependence of Electronic Spectra for Linear Anionic Carbon Clusters C_n^- (n = 4–17). *J. Comput. Chem.* **2012**, *33*, 93–102. [CrossRef] [PubMed]
22. Zhao, Y.; He, H.; Zhang, J.; Wang, L. Direct dynamics study of the hydrogen abstraction reaction of CF_3CH_2Cl + Cl -> CF_3CHCl + HCl. *Int. J. Chem. Kinet.* **2012**, *44*, 661–667. [CrossRef]
23. Fan, Y.; Wen, J.; Zhao, Y.; Wang, L. Theoretical study on the hydrogen abstraction reactions of CF_3CHFCF_3 and $CF_3CF_2CHF_2$ with X atoms (X = F, Cl, and Br). *J. Fluorine Chem.* **2013**, *150*, 39–45. [CrossRef]
24. Zhao, Y.; Guo, J.; Zhang, J. A theoretical study of electronic spectra in the linear cationic chains $NC_{2n+1}N^+$ (n = 1–6). *Chem. Phys.* **2011**, *386*, 23–28. [CrossRef]
25. Zhan, C.-G.; Iwata, S. Ab initio studies on the structures, vertical electron detachment energies, and stabilities of C_nP^- clusters. *J. Chem. Phys.* **1997**, *107*, 7323–7330. [CrossRef]
26. Sun, S.; Cao, Y.; Sun, Z.; Tang, Z.; Zheng, L. Experimental and Theoretical Studies on Carbon−Nitrogen Clusters $C_{2n}N_7^-$. *J. Phys. Chem. A* **2006**, *110*, 8064–8072. [CrossRef]
27. Tang, Z.; BelBruno, J.J.; Huang, R.; Zheng, L. Collision-induced dissociation and density functional study of the structures and energies of cyclic $C_{2n}N_5^-$ clusters. *J. Chem. Phys.* **2000**, *112*, 9276–9281. [CrossRef]
28. Li, G.; Xing, X.; Tang, Z. Structures and properties the lead-doped carbon clusters $PbC_n/PbC_n^+/PbC_n^-$ (n = 1–10). *J. Chem. Phys.* **2003**, *118*, 6884–6897. [CrossRef]
29. Zhang, C.-J.; Jiang, Z.-Y.; Wang, Y.-L.; Zhu, H.-Y. Structures and stabilities of GaC_n (n = 1–10) clusters. *Comput. Theor. Chem.* **2013**, *1004*, 12–17. [CrossRef]
30. Chen-Jun, Z.; Yang-Li, W.; Chao-Kang, C. Density functional theory of $InCn^+$ (n = 1–10) clusters. *Acta Phys. Sin.* **2018**, *67*, 113101. [CrossRef]
31. Wang, P.; Yan, S.-T.; Xu, H.-G.; Xu, X.-L.; Zheng, W.-J. Anion photoelectron spectroscopy and density functional theory studies of $AuCn^-/0$ (n = 3−8): Odd-even alternation in electron binding energies and structures. *Chin. J. Chem. Phys.* **2022**, *35*, 177–184. [CrossRef]
32. Zhang, C.; Xu, H.; Xu, X.-L.; Zheng, W.-J. Electronic structures, chemical bonds, and stabilities of $Ta_4C^-/0n$ (n = 0–4) clusters: Anion photoelectron spectroscopy and theoretical calculations. *Acta Phys. Sin.* **2021**, *70*, 023601. [CrossRef]
33. Freitas, A.; Azevedo, S.; Kaschny, J.R. Structural and electronic properties of linear carbon chains encapsulated by flattened nanotubes. *Phys. E-Low-Dimens. Syst. Nanostruct.* **2016**, *84*, 444–453. [CrossRef]
34. Rocha, R.A.; dos Santos, R.B.; Ribeiro Junior, L.A.; Aguiar, A.L. On the Stabilization of Carbynes Encapsulated in Penta-Graphene Nanotubes: A DFT Study. *J. Mol. Model.* **2021**, *27*, 318. [CrossRef]
35. Zhang, Y.; Su, Y.; Wang, L.; Kong, E.S.-W.; Chen, X.; Zhang, Y. A one-dimensional extremely covalent material: Monatomic carbon linear chain. *Nanoscale Res. Lett.* **2011**, *6*, 577. [CrossRef]
36. Yang, S.; Li, W.; Li, Y.F.; Chen, X.M.; Zhang, H.; Xu, B.Q.; Yang, B. Structural, electronic and catalytic properties of Ag_nSn_n (n = 2–14) clusters by density functional theory. *Phys. Chem. Chem. Phys.* **2022**, *24*, 26631–26641. [CrossRef] [PubMed]
37. Pascoli, G.; Lavendy, H. Theoretical Study of C_nP, C_nP^+, C_nP^- (n = 1–7) Clusters. *J. Phys. Chem. A* **1999**, *103*, 3518–3524. [CrossRef]
38. Pascoli, G.; Lavendy, H. Are C_nN^- clusters really bent? *Chem. Phys. Lett.* **1999**, *312*, 333–340. [CrossRef]
39. Frisch, M.J.; Trucks, G.W.; Schlegel, H.B.; Scuseria, G.E.; Robb, M.A.; Cheeseman, J.R.; Montgomery, J.A., Jr.; Vreven, T.K.; Kudin, K.N.; Burant, J.C.; et al. *Gaussian 03 Rev. A01*; Gaussian Inc.: Wallingford, CT, USA, 2004.
40. Pan, Y.; Yu, E. New insight into the structural and physical properties of AlH_3. *Int. J. Energ. Res.* **2022**, *46*, 19678–19685. [CrossRef]
41. Song, Z.; Zhao, B.; Wang, Q.; Cheng, P. Steering reduction and decomposition of peroxide compounds by interface interactions between MgO thin film and transition-metal support. *Appl. Surf. Sci.* **2018**, *459*, 812–821. [CrossRef]

42. Chen, S.; Pan, Y. Enhancing catalytic properties of noble metal@MoS_2/WS_2 heterojunction for the hydrogen evolution reaction. *Appl. Surf. Sci.* **2022**, *591*, 153168. [CrossRef]

43. Pan, Y. First-principles investigation of the effect of noble metals on the electronic and optical properties of GaN nitride. *Mat. Sci. Semicon. Proc.* **2022**, *151*, 107051. [CrossRef]

44. Zhou, Y.; Shao, X.J.; Lam, K.H.; Zheng, Y.; Zhao, L.Z.; Wang, K.D.; Zhao, J.Z.; Chen, F.M.; Hou, X.H. Symmetric Sodium-Ion Battery Based on Dual-Electron Reactions of NASICON-Structured $Na_3MnTi(PO_4)_3$ Material. *ACS Appl. Mater. Inter.* **2020**, *12*, 30328–30335. [CrossRef] [PubMed]

45. Xu, W.P.; Zhao, J.Z.; Xu, H. Adsorption Induced Indirect-to-Direct Band Gap Transition in Monolayer Blue Phosphorus. *J. Phys. Chem. C* **2018**, *122*, 15792–15798. [CrossRef]

46. Lee, C.; Yang, W.; Parr, R.G. Development of the Colle-Salvetti correlation-energy formula into a functional of the electron density. *Phys. Rev. B* **1988**, *37*, 785–789. [CrossRef] [PubMed]

47. Wu, J.Y.; Yan, H.; Zhong, A.G.; Chen, H.; Jin, Y.X.; Dai, G.L. Theoretical and conceptual DFT study of pnicogen-and halogen-bonded complexes of PH_2X—BrCl. *J. Mol. Model.* **2019**, *25*, 28. [CrossRef] [PubMed]

48. Zhu, H.Y.; Wu, J.Y.; Dai, G.L. Study on the halogen bond and pi-pi stacking interaction between fluoro substituted iodobenzene and pyrazine. *J. Mol. Model.* **2020**, *26*, 333. [CrossRef]

49. Wu, J.Y.; Yan, H.; Chen, H.; Jin, Y.X.; Zhong, A.G.; Wang, Z.X.; Dai, G.L. Three types of noncovalent interactions studied between pyrazine and XF. *J. Mol. Model.* **2022**, *28*, 15. [CrossRef]

50. Wu, J. Investigations into the nature of halogen-and hydrogen-bonding interactions of some heteroaromatic rings with dichlorine monoxide. *J. Mol. Model.* **2014**, *20*, 2424. [CrossRef]

51. Pascoli, G.; Lavendy, H. Geometrical structures of the phosphorus-doped carbon cluster cations C_nP^+ (n = 1–20). *Int. J. Mass Spectrom.* **1999**, *189*, 125–132. [CrossRef]

52. Pascoli, G.; Lavendy, H. Structures and energies of C_nSi^+ ($4 \leq n \leq 15$) silicon carbide clusters. *Int. J. Mass Spectrom.* **1998**, *173*, 41–54. [CrossRef]